Extension of Fourier-based techniques for ultrafast imaging in ultrasound with diverging waves

Miaomiao Zhang, François Varray, Adrien Besson, Rafael E. Carrillo, Magalie Viallon, Damien Garcia, Jean-Philippe Thiran, Denis Friboulet, Hervé Liebgott, and Olivier Bernard

***Abstract*—Ultrafast ultrasound imaging has become an intensive area of research thanks to its capability in reaching high frame rates. In this paper, we propose a scheme which allows the extension of the current Fourier-based techniques derived for planar acquisition to the reconstruction of sectorial scan with wide angle using diverging waves. The flexibility of the proposed formulation was assessed through two different Fourier-based techniques. The performance of the derived approaches was evaluated in terms of resolution and contrast from both simulations and in vitro experiments. Comparisons with the current state-of-the-art method illustrated the potential of the derived methods in producing competitive results with lower computational complexity when compared to the conventional Delay-And-Sum technique.**

***Index Terms*—Ultrafast imaging, Fourier-based method, diverging waves.**

I. Introduction

CONVENTIONAL ultrasound imaging is usually performed by scanning a medium using sequential focused or multi-focused beams, each firing allowing the reconstruction of one narrow sector of the final image [1], [2]. Assuming that the only limitation to the frame rate is the ultrasound wave propagation, the time needed to construct an image is thus proportional to the number of lines, the image depth and the speed of sound. Limitations of conventional approach appear when a large number of lines is required, or when the dynamics of the phenomena to be imaged is faster than the frame rate currently delivered by the ultrasound systems. 3D cardiac imaging is a typical example of such challenge since the number of lines to acquire for one volume becomes very large and the corresponding frame rate substantially decreases, with a typical value around 1 volume per second (vps) for the same image quality as in 2D or with values between 10 to 40 vps using dedicated strategies (*e.g.* slightly broadened transmission beams or ECG gating) but at the cost of the resolution and potential stitching artifacts [3].

Although frame rates around several tens of images per second are sufficient for real-time observation of cardiac morphology, the understanding of complex cardiac dynamics requires a significant increase of the temporal resolution. In order to reduce the number of transmissions, methods based on plane wave (PW) insonifications have been proposed. These approaches use PW to insonify the whole medium with one single emission. The backscattered echoes are then measured and post-processed to reconstruct simultaneously all lines of the image of interest [4]. The concept of broad field-of-view transmit beams with full parallel receive beamforming dates back to the late 90s, when Lu *et al.* developped a high frame rate imaging method based on limited diffraction beams [5], [6]. This method is based on the reconstruction of the Fourier spectrum of the object function. More recently, the same group proposed to extend this approach to steered plane waves (SPW) in transmission in order to reconstruct ultrasound images with wider field of view [7]. Garcia *et al.* proposed an f-k migration method for plane wave imaging based on the exploding reflector model used in exploration seismology [8]. This method also reconstructs the Fourier spectrum of the object function but with noticeable differences for the high lateral frequency components. One important shared property of the two above mentioned methods is that the Fourier spectrum of the object is sampled along the k_z axis direction with a lateral step proportional to the inverse of the pitch (distance between two consecutive active elements). As an alternative, Bernard *et al.* recently proposed in [9] a technique based on the Fourier slice theorem which samples the Fourier space radially. In a different manner, starting from PW in transmission, Montaldo *et al.* proposed a more conventional Delay-And-Sum (DAS) method applied in reception which allows the reconstruction of the image of interest directly from the space domain [10].

The use of these methods to reconstruct an ultrasound image from only one transmission comes up with an image quality (defined in terms of resolution and contrast) intrinsically lower than the one obtained with classical multi-line focused beamforming. To overcome this limitation, spatial coherent compounding has been used in many studies to improve image quality [6], [8], [10].

Based on the steering of several SPW, the concept of this technique is to uniformize focusing synthetically in the full image in transmission, as it is done in synthetic transmit aperture [11], but with a higher frame rate and/or a higher contrast depending on the transmission settings (*e.g.* number of firing elements, steering angles or number of PW). Although ultrafast imaging based on coherent compounding using SPW is a recent technique, it has been already applied in many ap-

O. Bernard, M. Zhang, F. Varray, M. Viallon, H. Liebgott and D. Friboulet are with the University of Lyon, CREATIS, CNRS UMR 5220, Inserm U1044, INSA-Lyon, University of Lyon 1, Villeurbanne, France. E-mail: olivier.bernard@creatis.insa-lyon.fr

A. Besson, J.P. Thiran and R.E. Carrillo are with the Signal Processing Laboratory (LTS5), Ecole polytechnique fédérale de Lausanne (EPFL), Lausanne, Switzerland.

J.P. Thiran is also with the Department of Radiology, University Hospital Center (CHUV) and University of Lausanne (UNIL), Lausanne, Switzerland.

M. Viallon is also with the University Hospital of Saint-Etienne, France.

D. Garcia is with the Research Unit of Biomechanics and Imaging in Cardiology, University of Montreal Hospital, Quebec H2X 0A9, Canada.

plications, such as transient elastography, pulse wave velocity imaging, flow imaging, shear wave imaging, ultrafast Doppler imaging and electromechanical wave imaging [10], [12]–[23].

PW compounding techniques become inefficient at large depths and for wide field of views since the overlap of the steered waves does not cover distant regions homogeneously. In such cases (*e.g.* in cardiac imaging) a broader wave is needed in emission in order to insonify a larger part of the medium of interest with a single transmit. In this context, Lu and Chen proposed to directly apply their PW reconstruction technique on the received signals generated from the transmission of diverging wave (DW) [24]. However, their method introduces geometrical distortions along the lateral direction. They thus proposed to restrict their method to the emission of DW with small angles (less than $15°$) to reduce these artifacts. Hasegawa *et al.* proposed to use DW compounding in transmission and parallel beamforming in reception to perform high frame rate imaging in 2D echocardiography [25]. In particular, the authors proposed to use several diverging beams with different directions to cover the entire medium. Contrary to this approach, Papadacci *et al.* proposed to use several DWs which individually insonify the entire field of view along with a compound strategy in order to improve the image quality [26]. Recently, Porée *et al.* developed an original coherent compounding approach with Doppler-based motion-compensation to generate high-quality cardiac images by DW imaging [27].

The above mentioned ultrafast imaging methods can be classified into two groups: the Fourier-based techniques where the received raw-data are used to reconstruct the Fourier spectrum of the object of interest [5], [8], [9] and the spatial-based approaches where the images are directly computed from the space domain [10], [25], [26]. The main advantage of the Fourier-based approaches concerns the computational complexity, this aspect having been investigated in several studies in the context of planar acquisition from SPW [8], [28]. In particular, the computational complexity of the DAS method proposed in [10] is equal to $O(n_e\, n_e\, n_s)$ and decreases to $O(n_e\, n_s \log(n_e\, n_s))$ for Fourier-based techniques [8] (n_e representing the number of transducer elements and n_s the number of samples of the beamformed signal).

Based on these observations, we introduce in this paper an explicit transformation which allows a direct extension of existing Fourier-based techniques derived for planar acquisition to the reconstruction of sectorial images with wide angles ($90°$). A first trial to validate this approach has been recently investigated in our previous work but restricted to the emission of a single DW and the use of one specific Fourier-based technique [29]. In comparison with this existing work, the novelties introduced in this paper are the following:

- We derived an explicit spatial transformation which allows the reconstruction of wide angle images from compounding scheme in emission.
- We showed that this new formulation allows a direct extension of two existing Fourier-based methods to sectorial acquisitions using a combination of DWs in transmission.
- We assessed the validity of the proposed method from both simulations and in vitro experiments. Its feasibility was also investigated in vivo from a human heart.

The remainder of the paper is organized as follows. In Section II, the proposed approach is described. The quality of the reconstructed images is then investigated in Section III. A discussion part is provided in Section IV while concluding remarks are given in Section V.

II. Methodology

In this section, we propose a formulation which allows a direct extension of the Fourier-based methods of Lu *et al.* [5] and Bernard *et al.* [9] to sectorial acquisitions using a combination of DWs in transmission. These two methods are well adapted to the formulation given below since the underlying image formation explicitly involves the same transducer for both transmission and reception. Contrary to these approaches, the method of Garcia *et al.* is based on the exploding reflector model, leading to approximations which are not adapted in this work (see [8] for more details).

A. Fourier-based techniques for planar acquisition

A brief summary of the Fourier-based techniques proposed by Lu *et al.* and Bernard *et al.* in the particular case of the transmission of one horizontal PW is given below. The reader is refered to [5] and [9] for more details.

1) Lu's method: Lu *et al.* first proposed in the late 90s a Fourier method for high frame rate imaging with limited diffraction beams (PW being a particular case) [5]. From the use of limited diffraction beams with normal incidence both in transmission and reception, the authors demonstrated that it is possible to reconstruct the Fourier spectrum of the object function from the following equation:

$$k_z = k + \sqrt{k^2 - k_x^2}\,, \tag{1}$$

where (k_x, k_z) corresponds to the wavenumbers of the object function and k is related to the temporal frequency of the raw-data by $k = 2\pi\, f/c$ (c being the speed of sound).

2) Bernard's method: more recently, Bernard *et al.* proposed a new formulation which expresses the problem of ultrasound image formation through the Fourier slice theorem [9]. Starting with a PW with normal incidence in transmission, and by using a SPW in reception with a given angle ξ_i, the authors demonstrated that the 1D Fourier transform of the sum of the received signals corresponds to a radial line with an angle equals to $\xi_i/2$ in the 2D Fourier spectrum of the insonified medium. In this way, by using a sequence of varying steered angles in reception, this technique allows from the transmission of one single PW to radially recover the Fourier space of the insonified medium based on the following fundamental relations (see Eq.(7) in [9]):

$$\left\{ \begin{array}{l} k_x \,=\, k\, \sin(\xi_i) \\ k_z \,=\, k\, (1 + \cos(\xi_i)) \end{array} \right. \tag{2}$$

where k is the same wavenumber as the one introduced in Lu's theory (Eq. (1)). Although the Fourier sampling scheme is different, it has been shown that Lu and Bernard methods reconstruct close Fourier spectrum, the only difference arising in the sampling density [9].

B. Extension of Fourier-based techniques to sectorial imaging

The key idea of this part is to establish an isomorphism in terms of travel time when either a DW or a PW is used in transmission as illustrated in Fig. 1. Indeed, such a relation would allow the reconstruction of a sectorial image from a DW using the same formalism as the one derived for planar acquisition. Isomorphism between travel times has been first proposed by Garcia *et al.* to adapt the seismic Stolt's migration technique to ultrasound plane wave imaging [8]. Let us define a probe located at $z = 0$, centered at $x = 0$ and where each transducer element E is positioned at $(x_E, 0)$. Getting inspired by the recent works performed on ultrasfast imaging for sectorial acquisition [25]–[27], we propose in this work to use DW in order to insonify the entire field of view with one transmission. Such a wave is obtained through the excitation of a virtual source located behind the probe and placed at (x_v, z_v), where $x_v \in [-L/2, L/2]$ (L being the width of the probe), and $z_v \leq 0$ is determined by the chosen angular aperture α and the sub-aperture width D as:

$$z_v = -\frac{D/2}{\tan(\alpha)} \tag{3}$$

The transmit delays Δ_E associated with the virtual source position and computed for each transducer element are then calculated as:

$$\Delta_E = \left(\sqrt{(x_E - x_v)^2 + z_v^2} + z_v\right) / c \tag{4}$$

where the second term in the brackets is used as an offset to ensure that the smallest transmitted delay is null. In this context, the travel time of a DW to reach a point scatterer positioned at (x_d, z_d) in the medium and to come back to a transducer element placed at $(x_E, 0)$ is given by:

$$\tau_d(x_E) = \left(\sqrt{(x_d - x_v)^2 + (z_d - z_v)^2} + z_v + \sqrt{(x_d - x_E)^2 + z_d^2}\right) / c \tag{5}$$

In the case of PW with normal incidence, the travel time involved to reach a point scatterer (x_p, z_p) and to come back to the same transducer element $(x_E, 0)$ is given by:

$$\tau_p(x_E) = \left(z_p + \sqrt{(x_p - x_E)^2 + z_p^2}\right) / c \tag{6}$$

By equating the first order Taylor approximation of (5) and (6) at $x_E = x_v$, the following relation between (x_d, z_d) and (x_p, z_p) can be derived:

$$\begin{cases} x_p \approx \frac{(x_d - x_v)\left(\sqrt{(x_d - x_v)^2 + (z_d - z_v)^2} + z_v\right)}{z_d + \sqrt{(x_d - x_v)^2 + z_d^2}} \\ \qquad + \frac{(x_d - x_v)\sqrt{(x_d - x_v)^2 + z_d^2}}{z_d + \sqrt{(x_d - x_v)^2 + z_d^2}} + x_v \\ z_p \approx \frac{z_d\left(\sqrt{(x_d - x_v)^2 + (z_d - z_v)^2} + z_v + \sqrt{(x_d - x_v)^2 + z_d^2}\right)}{z_d + \sqrt{(x_d - x_v)^2 + z_d^2}} \end{cases} \tag{7}$$

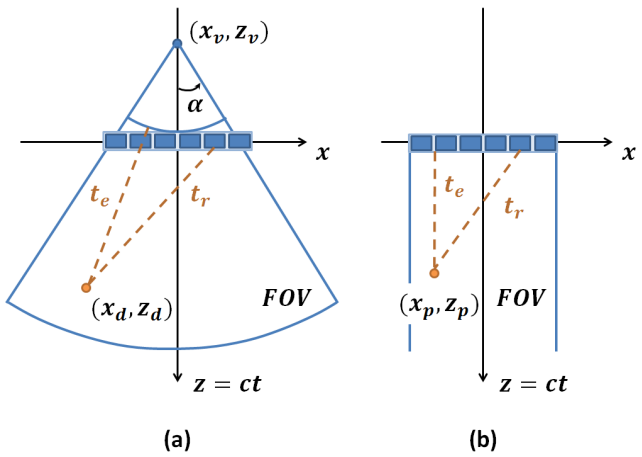

Fig. 1. Illustration of the travel time (t_e and t_r) involved when either (a) a DW or (b) PW is used in transmission. In both cases, $(t_e + t_r)$ corresponds to the time needed by the insonifying wave to reach a scatterer (orange dot) and then come back to a specific transducer element.

and

$$\begin{cases} x_d \approx \frac{1}{2}\frac{(x_p - x_v)\left(z_v^2 - \left(z_p + \sqrt{(x_p - x_v)^2 + z_p^2} - z_v\right)^2\right)}{z_v\, z_p - \left(z_p + \sqrt{(x_p - x_v)^2 + z_p^2} - z_v\right)\left(\sqrt{(x_p - x_v)^2 + z_p^2}\right)} \\ \qquad + x_v \\ z_d \approx \frac{1}{2}\frac{z_p\left(z_v^2 - \left(z_p + \sqrt{(x_p - x_v)^2 + z_p^2} - z_v\right)^2\right)}{z_v\, z_p - \left(z_p + \sqrt{(x_p - x_v)^2 + z_p^2} - z_v\right)\left(\sqrt{(x_p - x_v)^2 + z_p^2}\right)} \end{cases} \tag{8}$$

From Eq. (7) and (8) the following algorithm is thus proposed to reconstruct a sectorial image: *i)* transmission of a DW using a standard phased-array; *ii)* from the received echo, application of a standard Fourier-based technique derived for PW. From Eq. (7), one can see that the output of this step will reconstruct the desired ultrasound image but expressed in the (x_p, z_p) coordinate system; *iii)* application of the spatial transformation given through Eq. (8) which allows expressing the reconstructed image in the conventional cartesian space.

C. Correctness of the proposed formulation

It is worth pointing out that Eq. (7) and (8) have been obtained for the particular case $x_E = x_v$, meaning that the equivalence between the travel time of equation (5) and (6) is exact only near the region defined by $x = x_v$, where the Taylor approximation remains valid. We thus investigated the error in terms of travel time difference for the special case $x_v = 0$ when the relation (7) and (8) are used for each point in the medium. More precisely, for each point (x_d, z_d) of the medium, we first computed the set of travel times $\{\tau_d(i)\}_{i \in [1,N]}$ from the virtual source point $(0, z_v)$ to (x_d, z_d) back to each transducer element i of the probe (N being the number of elements). We then derived the corresponding (x_p, z_p) points and compute the set of travel times

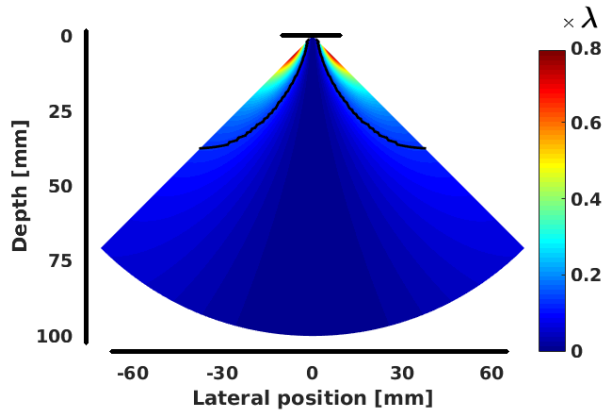

Fig. 2. Error map derived from the travel time equivalence between a sectorial acquisition using DW and the equivalent PW imaging after the application of the proposed spatial transformation. The computed error is expressed relatively to the wavelength used in the experiments. The black line on the top of the figure models the transducer location while the axis origin is located at the center of the probe. The two black curves drawn inside the error map represent the boundary of the region at the edge of the image where the maximum error is higher than $\lambda/8$

$\{\tau_p(i)\}_{i\in[1,N]}$ from the probe to (x_p, z_p) back to each transducer element i. In the case of a perfect equivalence between the two systems, the set of the pair-wise difference $\tau_d(i)-\tau_p(i)$ over the probe element should be zero. Fig. 2 shows the corresponding maximum value (*i.e.* $\max_i(\tau_d(i)-\tau_p(i))$) computed for each point of the medium in terms of the wavelength λ. From this figure, one may first observe that there is no difference in terms of travel time at the center of the probe and this error increases at the edge of the image. The maximum error appears in the near field (depth lower than 1-cm) at the edges of the image with a value around $0.8 \times \lambda$. This figure also allows the assessment of the potential defocusing effect induced by the proposed formulation. Indeed, each value displayed in figure 2 corresponds to the maximum of the error between the two systems computed over the full aperture. Since for each reconstructed point, the travel time error for most of the elements is below $\lambda/8$ (which is the commonly accepted value under which errors in travel distances can be neglected), it reveals the marginal effect of defocusing during the beamforming process. A more detailed investigation of this particular aspect is given in the online supplementary materials. Finally, it is worth pointing out that the negliged effect of defocusing also justifies the correct reconstruction of the point positioning after the spatial transformation. This aspect will be further investigated in Section III-A1.

D. Summary and pratical implementation

The formulations introduced in section II-B allow the reconstructiion of an image from the transmission of a diverging wave with a virtual source positioned at any (x_v, z_v). Thus, by reproducing the scheme proposed in [26], *i.e.* emitting several diverging waves with virtual sources positioned at $z_v = -D/(2\tan(\alpha))$ and for different x_v values, our formalism can be used to reconstruct wide field of view ultrasound images with efficient compounding scheme. The implementation of the procedure for sectorial imaging from the two Fourier-based techniques described in Section II-A can thus be summarized as follows:

1) Transmit one or several DWs to insonify the medium. In particular, for a virtual source positioned at (x_v, z_v), the corresponding DW is generated by applying the delays given in Eq. (4) for each transducer element.
2) Receive simultaneously on each transducer the backscattered echoes. This step allows the collection of a 2D matrix for each DW insonification.
3) Apply one particular Fourier-based reconstruction method designed for PW (i.e. Lu or Bernard's method) on each received 2D matrix. This step allows the reconstruction of an RF image which is expressed in a space with coordinates (x_p, z_p).
4) Apply the spatial transformation given in Eq. (8) to reconstruct the corresponding RF image in the Cartesian space with coordinates (x_d, z_d).
5) If successive DWs are used to perform coherent compounding, repeat steps 3 and 4 for each firing and average all the reconstructed RF images to get the final compounded image.

Note that step 3) implies the interpolation of the collected data on a regular grid in the Fourier domain in order to compute the reconstructed image using a regular 2D inverse Fourier transform. Such interpolation is an old topic which has been widely studied in the literature [30]–[32]. In particular, as described in details in [31], the linear interpolation applied in k-space leads to the multiplication of the real image by a squared sinc function. This results in a decrease of the intensity of the current reconstructed image along depth. To reduce this artifact, we applied a depth-varying intensity correction for the Fourier-based techniques. An intensity correction of 0.5-dB/MHz/cm was used.

E. Experiments

The performance of the proposed transformation associated with the Fourier-based techniques proposed by Bernard and Lu was evaluated from both numerical and *in vitro* phantoms, as well as from in vivo data from a cardiac acquisition.

1) Acquisition protocol: the same standard phased-array probe of 64 elements with a center frequency of 2.5-MHz (100% bandwidth), 0.32-mm pitch, 13-mm height and 60-mm elevation focus was used for all the tests. No apodization was used in transmission or reception. The imaging depth was set to 100-mm. For all the tests, the two extended Fourier methods were compared with the current state-of-the-art spatial-based method of Papadacci *et al.* Each reconstructed image was obtained from the following protocol: i) raw-data signals were acquired using DW with different virtual source point positions; ii) those signals were processed either following the two Fourier based methods described above or using the method of Papadacci *et al.* to obtain the compounded RF image; iii) the corresponding envelope image was derived through a Hilbert transform and normalized; iv) the envelope image was then gamma-compressed using $\gamma = 0.3$ as in [8]

and finally converted to 8-bit grayscale to get the B-mode image.

2) Transmission scheme: for comparison purposes and because of its efficiency, we used the same transmission scheme as the one proposed in [26]. Each DW involved in transmission was emitted from a virtual source point with an angular aperture of $90°$ and a sub-aperture width composed of 21 elements. For a single transmission, the virtual source was placed at the center of the probe. For three transmissions, the two others sources were placed near the edges of the transducer (*i.e.* at $x_v = [-6.7, 0, 6.7]$-mm). For more than three transmissions, the additional virtual sources were uniformly distributed (*i.e.* at $x_v = [-6.7, -3.35, 0, 3.35, 6.7]$-mm for 5 transmissions in our experiments). The number of transmitted DWs varied from 1 to 25, providing a frame rate between 7700 and 308 frame per second (fps).

3) Evaluation metrics: the image quality was assessed from the lateral resolution and the image contrast metrics. The contrast was measured from the B-mode images using the following classical contrast ratio (CR) [33]:

$$CR = 20 \log_{10} \frac{|\mu_t - \mu_b|}{\sqrt{(\sigma_t^2 + \sigma_b^2)/2}}, \tag{9}$$

where μ_t and μ_b (σ_t^2 and σ_b^2) are the means (variances) of gray levels in the targets and the surrounding background.

4) Numerical simulations: the conceptual correctness of the proposed spatial transformation was first investigated from a simple synthetic phantom composed of a discrete set of point scatterers (Fig. 4). The same phantom was also used to evaluate the quality of the reconstructed images through the lateral resolution. The corresponding values were measured as the full width at half maximum of the point spread function associated to the points located at 20-mm, 40-mm, 60-mm and 80-mm in the image. The image contrast was investigated from another phantom composed of a medium with high density of scatterers (20 per resolution cell) with two anechoic cysts of diameter 8-mm lying at 40 and 80-mm depth, respectively. For all the numerical simulations, the corresponding raw-data were generated using Field II [34], [35].

5) In vitro experiments: the in vitro experiments were performed with a Verasonics research scanner (V-256, Verasonics Inc., Redmond, WA) and a 2.5 MHz phased-array transducer (ATL P4-2, 64 elements). The CIRS tissue-mimicking phantom displayed in Fig. 3 was used for the in vitro experiments. The lateral resolution was first investigated from the acquisition centered on the 0.1-mm nylon monofilament targets positioned at 20-mm, 40-mm, 60-mm and 80-mm. The performance in terms of contrast was then measured from the hyperechoic cyst presents at 40-mm depth.

6) In vivo experiments: the in vivo experiments were performed with a Verasonics research scanner (V-1-128, Verasonics Inc., Redmond, WA) and a 2.5 MHz phased-array transducer (ATL P4-2, 64 elements). Very recently, Porée *et al.* have introduced a scheme for coherent compounding of tilted DWs which has been validated in cardiac imaging [27].

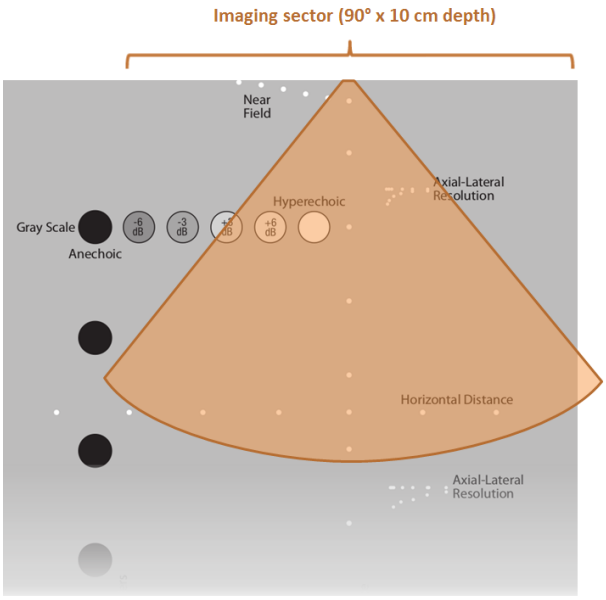

Fig. 3. Schematic diagram of the CIRS tissue-mimicking phantom (model: 054GS) with the corresponding imaging sector used in the DWs experiments.

In particular, to deal with high myocardium velocities, the authors have proposed to use a triangle transmit sequence of DWs, combined with tissue Doppler imaging to perform motion compensation (MoCo). In order to assess the ability of our approach to deal with in vivo data, we applied the exact same transmission scheme as the one described in [27] to reconstruct a cardiac sequence with and without motion compensation. In particular, we used 32 DWs in transmission (tilted from $-25°$ to $+25°$ with a triangle strategy) for the reconstruction of each frame of the final sequence. The cardiac data from Porée *et al.* [27] were reanalyzed as follows: *i)* apply the triangle transmit sequence of DWs given in [27], *ii)* for each firing, reconstruct a beamformed sectorial image using the extension of Lu's method; *iii)* apply the MoCo algorithm described in [27] on each of the image obtained at the previous step; *iv)* perform the compounding on the corrected images; *v)* repeat this process for each frame of the sequence.

III. Results

A. Numerical Simulations

1) Validation of the proposed framework: Fig. 4 displays the images reconstructed from the algorithm described in section II-D associated with the Fourier-based method of Bernard (Fig. 4a and 4b) and Lu (Fig. 4c) as well as the image reconstructed by the method of Papadacci *et al.* (Fig. 4d). The red circles correspond to the real position of the scatterers. From these figures, it can be seen that the proposed transformation allows the reconstruction of all the scatterers with the correct position whatever the chosen Fourier-based technique. This illustrates the marginal effect of the error map presented in section II-C and validates the flexibility of the proposed approach.

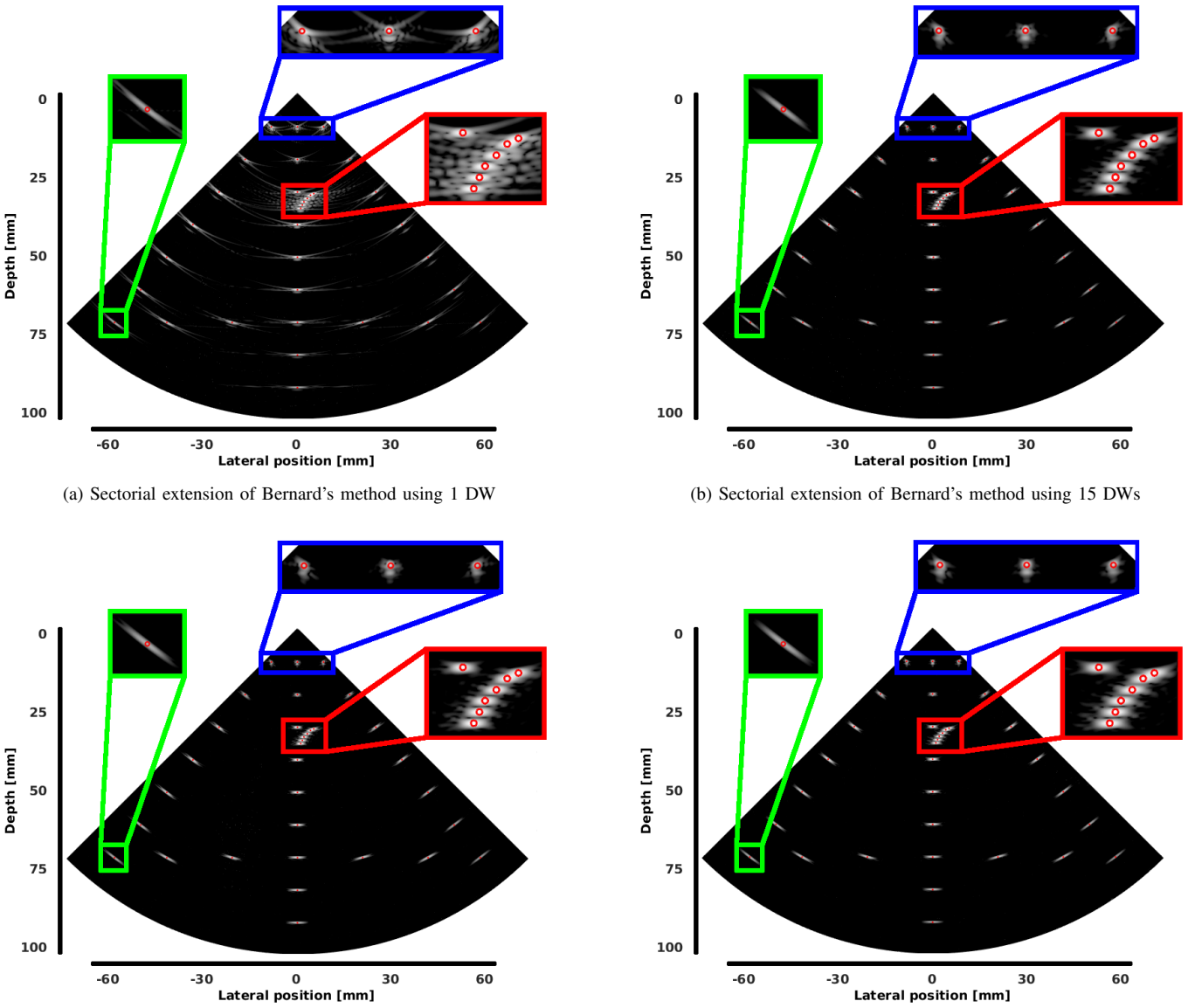

(a) Sectorial extension of Bernard's method using 1 DW

(b) Sectorial extension of Bernard's method using 15 DWs

(c) Sectorial extension of Lu's method using 15 DWs

(d) Papadacci's method using 15 DWs

Fig. 4. Synthetic phantom reconstructed from the extension of the Fourier-based methods of Bernard *et al.* and Lu *et al.* as well as the method of Papadacci *et al.* The red points correspond to the real position of the scatterers involved in the simulation.

2) Lateral resolution: Fig. 5a investigates the influence of the number of DWs on the lateral resolution using the different reconstruction techniques and for the different depths at the middle of the image (azimuth angle of $0°$). First, it can be seen that the 3 methods produce similar image quality whatever the depth and the number of DWs. In particular, it can be observed that the lateral resolution improves quickly for 3 DWs and then tends to stabilize to the optimal value, *i.e.* around 0.8-mm at 20-mm depth, 1.4-mm at 40-mm depth, 2.0-mm at 60-mm depth and 2.7-mm at 80-mm depth. It is also important to note that, for each depth, the lateral resolution tends to degrade a little bit after the compounding of 3 DWs. This behavior can be explained by the chosen transmission scheme. Indeed, in the particular case of a monochromatic far-field approximation at a focal distance F, the width W of the main lobe corresponding to a coherent summation of N DWs ($N > 1$) is in the order of (see Eq. (4) in [26]):

$$W = 2\,\frac{\lambda F}{W_{va}}\,\frac{N-1}{N} \tag{10}$$

where $\lambda = 2\pi/k$ and W_{va} corresponds to the width of the virtual array which is considered as fixed in this study. Based on this equation, we display in Fig. 6 the evolution of the approximation of the full width at half-maximum from the probe settings used in our simulations at a focal distance of 60-mm. From this figure, one can see that the theoretical evolution of this measure is consistent with the lateral resolution measured in simulations.

Fig. 5b investigates the influence of the number of DW on the lateral resolution using the different reconstruction

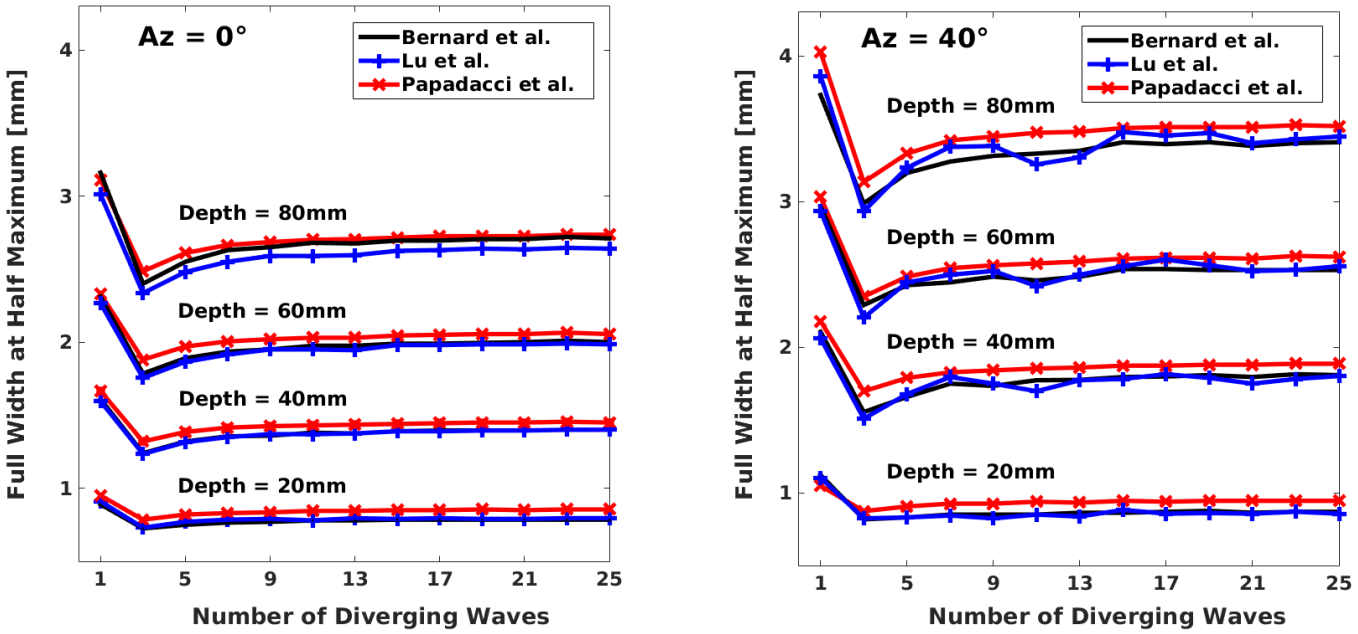

(a) (b)

Fig. 5. Numerical phantom - lateral resolution measurements as a function of the number of DWs computed at 20-mm, 40-mm, 60-mm and 80-mm at (a) the middle of the image (azimuth angle of $0°$) and (b) at the edge of the image (azimuth angle of $40°$).

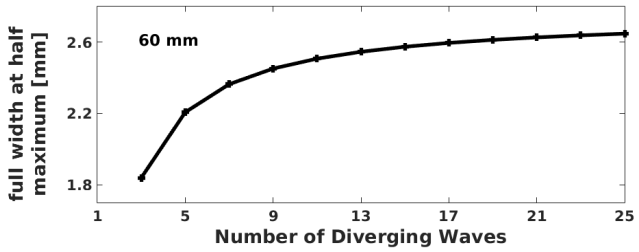

Fig. 6. Approximation of the full width at half maximum of the main lobe corresponding to the coherent summation of DWs in the case of a monochromatic far-field at a focal distance of 60-mm.

techniques and for different depths at the edge of the image (azimuth angle of $40°$). As for the middle case, it can be seen that the 3 methods produce similar image quality whatever the depth and the number of the involved DWs. It is also interesting to note that the lateral resolution (computed along the azimuth direction for consistency) degrades with the azimuth angle. For instance, at 80-mm depth, the lateral resolution goes from values around 2.7-mm at the middle of the image to values around 3.4-mm at the edge. This phenomenon can be explained by the fact that the region where the different DWs contribute to the image pixels is optimal at the middle of the image, leading to a better image resolution. The limited opening angle of the effective aperture may also reinforce this phenomenon. Finally, it can be observed from Fig. 5a and 5b that the difference in terms of lateral resolution between Papadacci's method and the Fourier based methods varies in average from 0.06-mm (at 20-mm depth) to 0.10-mm (at 80-mm), which corresponds of a maximum difference lower than $\lambda/6$. Since this difference is much lower than half of the wavelength, this phenomenon may be considered as negligible.

3) Image contrast: Fig. 7a displays the CR values measured for two different depths at the middle of the image (azimuth angle of $0°$) for each compounding experiment. The three methods yield very close results, the CR measurements showing same tendency with an increasing number of DW and with better CR scores at 40-mm. This can be easily explained by the intrinsic decrease of the transmit ultrasound pressure with depth which inevitably induces lower contrast. It is also interesting to note that for more than 15 DWs, the image contrast tends to stabilize to the optimal value for all methods, which is consistent with the results provided in [26]. Finally, Fig. 7b to 7d display the images reconstructed with the three different methods using 15 DWs. These results illustrate visually the closeness in terms of image quality and speckle definition of the images reconstructed from the proposed extension of the Fourier-based techniques and the spatial-based method of Papadacci *et al.*

Fig. 8 displays the CR values measured for two different depths at the edge of the image (azimuth angle of $40°$). As for the cysts in the middle, it can be seen that the 3 methods yield very similar image quality whatever the depth and the number of involved DW. It is of importance to note that the image contrast decreases a little bit with the azimuth angle. For instance, at 40-mm depth, the CR decreases from values around 13-dB at the middle of the image down to values around 10-dB at the edge.

B. In vitro and in vivo experiments

1) Lateral resolution: Fig. 9 illustrates the impact of DW compounding number on the lateral resolution for the different

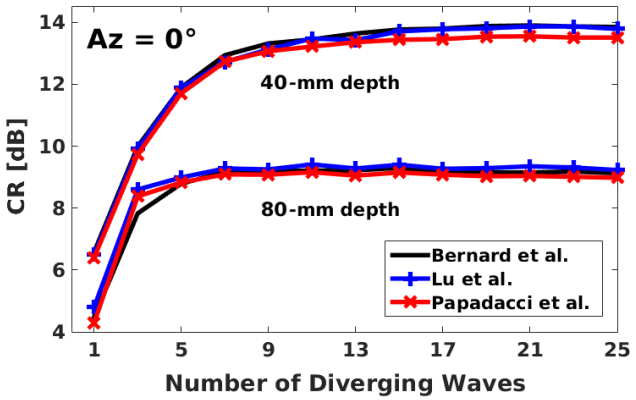

(a) Contrast ratio measurements for different depths

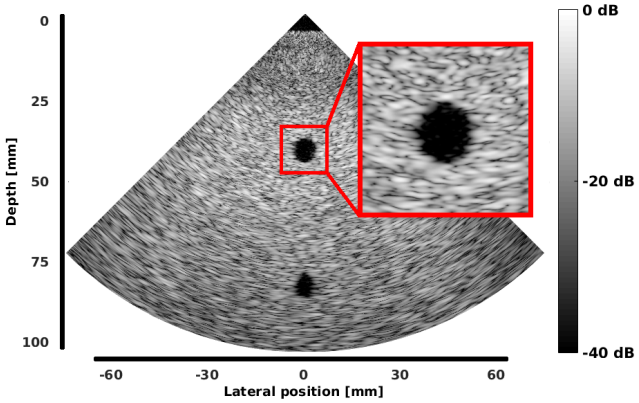

(b) Sectorial extension of Bernard's method

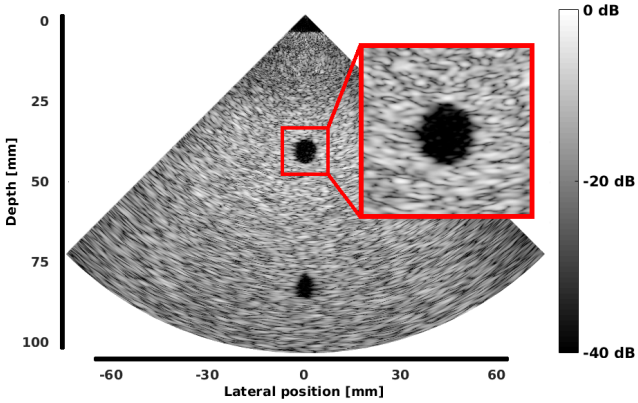

(c) Sectorial extension of Lu's method

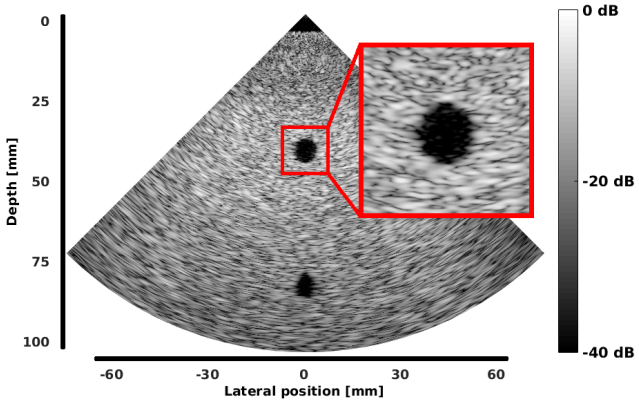

(d) Papadacci's method

Fig. 7. Numerical phantom - (a) contrast ratio measurements computed at the middle of the image (azimuth angle of 0°) as a function of the number of DWs. B-mode images reconstructed from (b) the proposed extension of Bernard's method, (c) the proposed extension of Lu's method and (d) the spatial-based method of Papadacci using 15 DWs with coherent compounding.

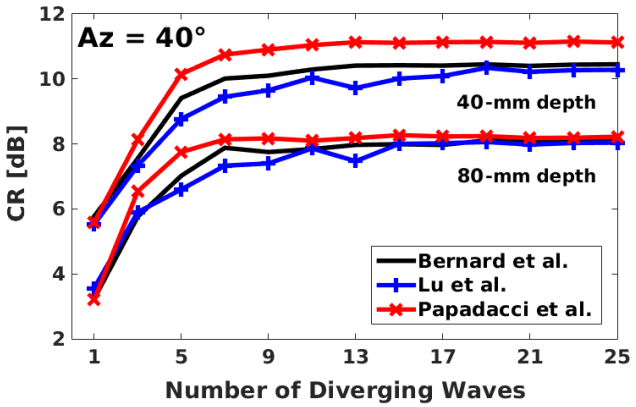

(a) Contrast ratio measurements for different depths

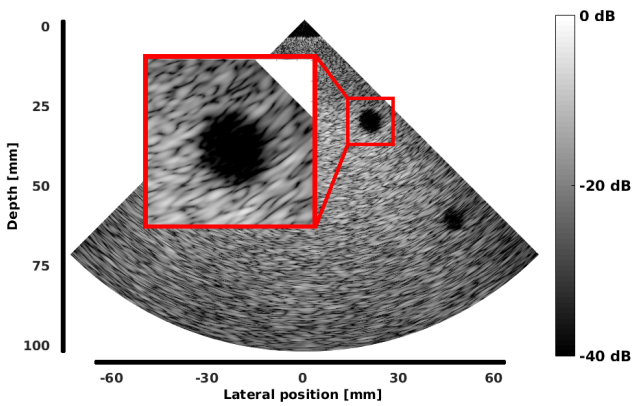

(b) Sectorial extension of Bernard's method

Fig. 8. Numerical phantom - (a) contrast ratio measurements computed at the edge of the image (azimuth angle of 40°) as a function of the number of DWs. B-mode images reconstructed from (b) the proposed extension of Bernard's method using 15 DWs with coherent compounding.

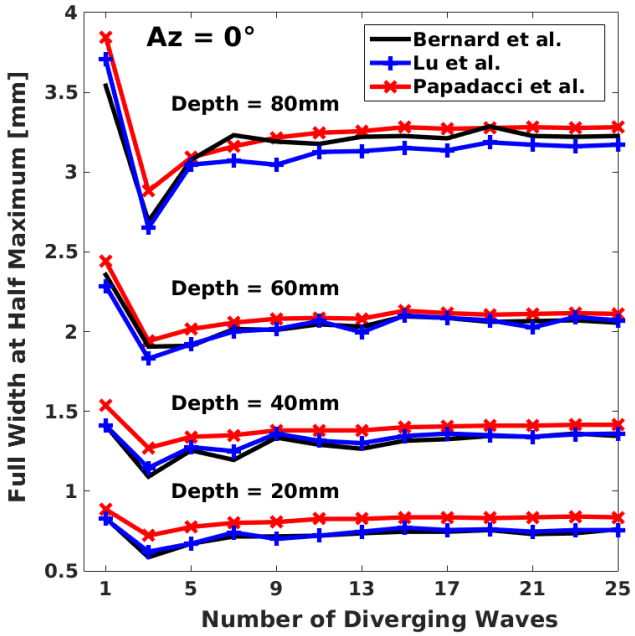

Fig. 9. Experimental acquisition - lateral resolution measurements computed at the middle of the image (azimuth angle of 0°) as a function of the number of DWs computed at 20-mm, 40-mm, 60-mm and 80-mm.

reconstruction techniques and for the different depths. One can first see that all the experimental results are consistent with what have been previously observed from simulations, both in terms of tendency and measured values. Indeed, for all the methods, the lateral resolution improved quickly for 3 DWs and then tended to stabilize to the optimal value, *i.e.* around 0.8-mm at 20-mm depth, 1.4-mm at 40-mm depth, 2.1-mm at 60-mm depth and 3.2-mm at 80-mm depth. Moreover, it is worth pointing out that at each depth, the different methods reached the optimal lateral resolution values for the transmission of 15 DWs, leading to an optimal frame rate of 855 fps.

2) Image contrast: we investigated in Fig. 10 the quality of the reconstructed images in terms of contrast. In particular, Fig. 10a displays the CR values measured at 40-mm depth for each compounding experiment. From the corresponding graph, it can be observed that the three methods yield very close results. The CR measurements involve same tendency over the increase of the number of DW. The optimal CR values are reached in all cases after the transmission of 15 DW (frame rate of 855 fps), which is in accordance with the simulation results we obtained in Section III-A3. Fig. 10b to 10d display the reconstructed B-mode images obtained using 15 DW with coherent compounding. As in simulations, these results illustrate visually the closeness in terms of image quality and speckle definition of the images produced by different methods. It is also interesting to note that the decrease of the intensity observed at the two borders of the image can be explained, on the left side, by the presence of a structure with high reflectivity (due to an unexpected flaw present in the CIRS phantom we used at the interface between the background and the hyperechoic cyst of +3dB) which produces classical ultrasound shadow and, on the right side, by the physical limit of the CIRS phantom which induces reverberation phenomenon. Finally, the limited opening angle of the transducer elements and the limited opening angle of the effective aperture may be additional causes responsible for the observed decrease of intensity at the edges.

3) In vivo experiment: Fig. 11 displays one particular frame of the full sequence we reconstructed from a real acquisition performed on a healthy volunteer with and without motion compensation, as described in section II-E6. The transmission scheme used during the acquisition process allowed us to compute a B-mode sequence of the whole left and right ventricles at high frame rate (250 fps). This result demonstrates the feasibility of the proposed formulation in a real setting, as well as its flexibility, since we could easily integrate the motion compensation framework proposed by Porée *et al.* [27].

IV. Discussion

A. Fourier-based methods of sectorial imaging

We proposed in this study an explicit transformation which allows the extension of existing Fourier-based approaches, initially proposed for planar acquisition, to the reconstruction of sectorial images with wide angle using DW. The proposed formulation was evaluated through the extension of two Fourier-based techniques, *i.e.* the one proposed by Lu *et al.* which samples the Fourier space along the k_z axis direction and the one of Bernard *et al.* which samples the Fourier space radially. Results obtained from both simulations and experiments revealed that the two extended Fourier-based approaches reconstruct images with comparable quality as it is the case for planar acquisition, the introduced spatial transform having no effect on their relative behavior. More importantly, we also demonstrated in this study that the proposed extended Fourier-based approaches produce competitive results compared to the state-of-the art method proposed by Papadacci *et al.* both in terms of lateral resolution and image contrast.

Although the proposed transformation has been specifically designed for the transmission scheme described in [26] (*i.e.* the virtual source point of each DW lies on a horizontal line positioned behind the probe), our approach can also be easily used for other strategies like, for instance, the steered diverging waves presented in [25]. In the case of SDW of angle θ, the second term z_v of Eq. (4) has to be simply replaced by $-\min_E \sqrt{(x_E - x_v)^2 + z_v^2}$ to ensure that the smallest transmit delay is null. The same reasoning then holds to derivate the akin spatial transformation. The corresponding equations have been used to produce the results given in Section III-B3.

B. Computational complexity

One strong interest of Fourier-based techniques for sectorial acquisition is a potential reduction of the computational complexity compared to the conventional DAS method. To determine the computational complexity of the proposed extension of Lu and Bernard methods, let n_e denotes the number of elements that compose the transducer (in general 64, 128 or 192), n_s the number of time samples (typically in the range

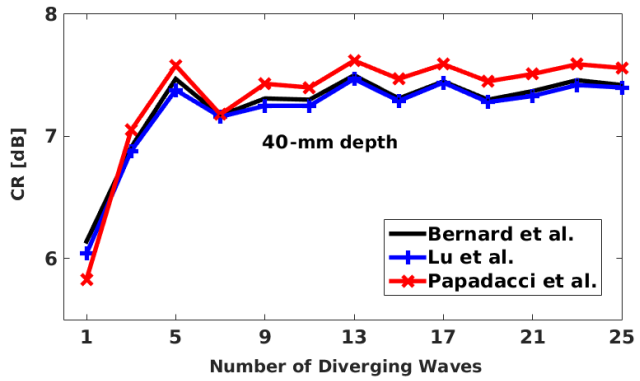

(a) Contrast ratio measurements

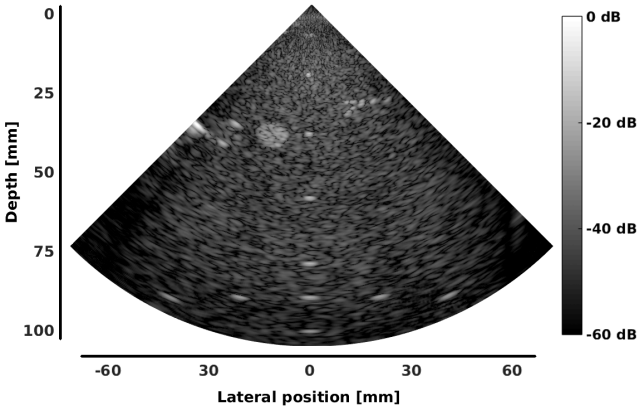

(b) Sectorial extension of Bernard's method

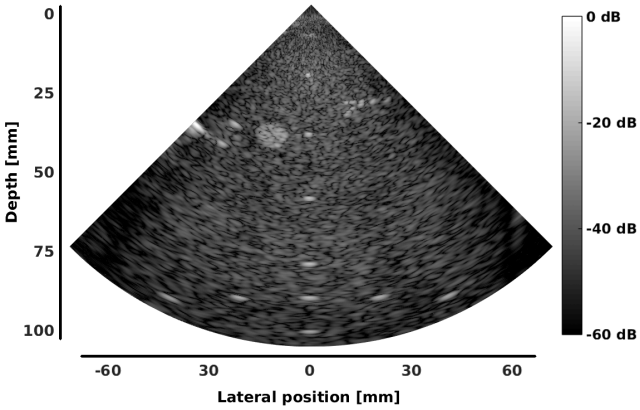

(c) Sectorial extension of Lu's method

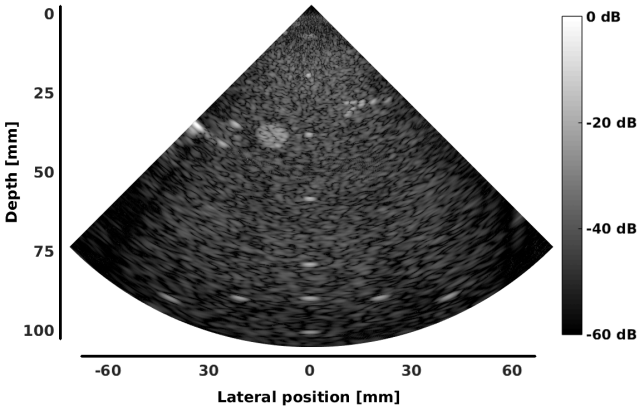

(d) Papadacci's method

Fig. 10. Real acquisition - (a) Contrast ratio measurements as a function of the number of DWs. B-mode images reconstructed from (b) the proposed extension of Bernard's method, (c) the proposed extension of Lu's method and (d) the spatial-based method of Papadacci using 15 DWs with coherent compounding.

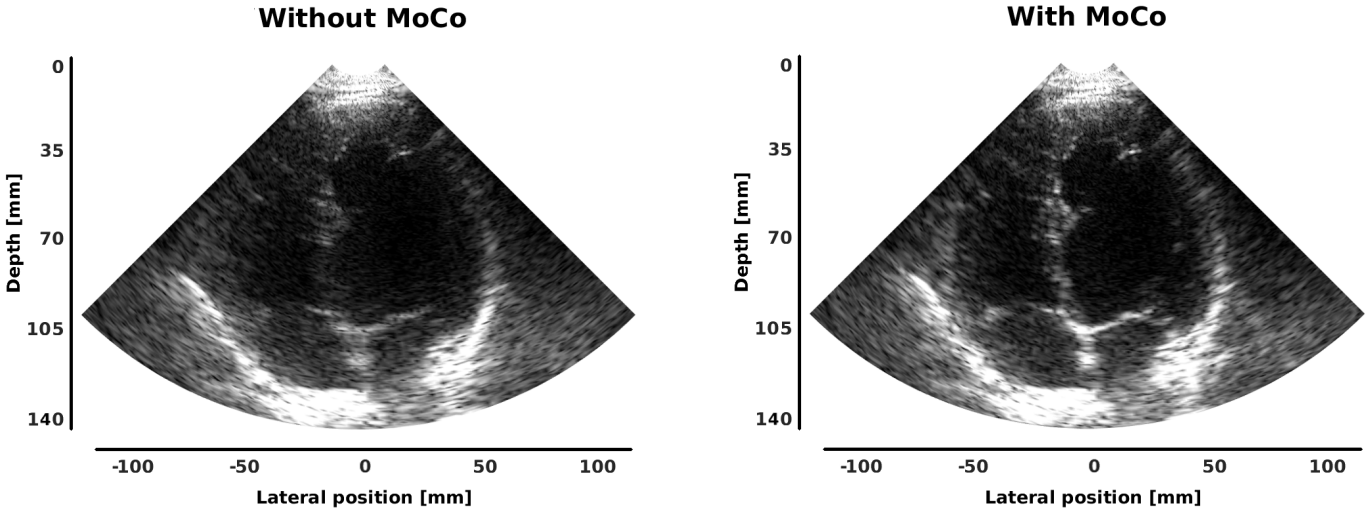

Fig. 11. Motion compensation for high frame rate echocardiography of the left ventricle using the sectorial extension of Lu's method. Each frame has been reconstructed from the transmission of 32 DWs (tilted from -25° to $+25^\circ$ with a triangle strategy as described in [27]). Online movies are also available in the supplementary materials. The data from Porée *et al.* [27] were reanalyzed with the technique described in the present paper.

1000-3000), n_x the number of samples along the x-axis for the reconstructed image (typically between 100 and 500) and n_ξ the number of angles over two used in reception for Bernard's method (the ratio of 2 being explained by the use of half of the spectrum). This value was fixed to 85 in our experiments, the reader is refered to [9] for more details.

Complexity of Papadacci's method: the DAS method proposed by Papadacci *et al.* must retrieve $\lambda\,(n_x\,n_s\,n_e)$ interpolated data and perform $\lambda\,(n_x\,n_s)$ summations over n_e, λ being the ratio between the scanned sectorial area and the corresponding encompassing rectangle (with dimensions $n_x\,n_s$). For an angular aperture of $90°$, λ is defined between $[0.5, 1]$. The computational complexity of the method of Papadacci *et al.* thus corresponds to $O(n_x\,n_s\,n_e)$.

Complexity of the proposed extension of Lu's method: the sectorial extension of Lu's method requires two 2-D FFTs (complexity of $O(n_x\,n_s\,\log(n_x\,n_s))$) and two times the computation of $(n_x\,n_s)$ interpolated values (one for the regridding step performed in the Fourier space and one for the spatial transformation introduced in this work). The computational complexity of the extension of Lu's method thus reduces to $O(n_x\,n_s\,\log(n_x\,n_s))$ compared to the method of Papadacci.

Complexity of the proposed extension of Bernard's method: the sectorial extension of Bernard's method requires n_e 1-D FFTs (complexity of $O(n_e\,n_s\,log(n_s))$), one 2D FFT (complexity of $O(n_x\,n_s\,\log(n_x\,n_s))$), the computation of $(n_\xi\,n_s\,n_e)$ multiplications for the delays applied in reception and two times the computation of $(n_x\,n_s)$ interpolated values (one for the regridding step performed in the Fourier space and one for the spatial transformation introduced in this work). The computational complexity of the extension of Bernard's method thus corresponds to $O(n_\xi\,n_s\,n_e)$, making the extension of this method less attractive than for the extension of Lu's method.

C. Extension to temporal acquisitions with tissue motion

Tissue motion is an important source of artifact in ultrafast imaging. In particular, when the motion of the structures of interest between two consecutive firings is higher than $\lambda/8$, it is common to observe a weakening of the compounding effect if no particular strategy is applied. Several approaches have thus been proposed to tackle this problem, both on PW [36] and DW [27]. In this paper, we showed the feasibility of the application of the motion compensation algorithm developed in [27] on the images reconstructed from the proposed approach. This shows the accuracy of our technique and validates further the marginal effect of the error map presented in section II-C.

D. Perspectives

One potential strong interest of the Fourier-based method compared to the DAS technique concerns its lower computational complexity. In the particular case of sectorial reconstruction, we have shown that the computational ratio between the sectorial extension of Lu's method and the standard DAS technique is of the order $n_e\,/\,\log(n_x\,n_s)$. Although the proposed transformation has been derived for 2D, it can be easily extended to 3D. To this end, one has to take into account the y-coordinate in the travel time equations of the PW (Eq. 6) and the DW (Eq. 5). By equating the first order Taylor approximation at $x_E = x_v$ and $y_E = y_v$, one can obtain the corresponding spatial transformation between (x_p, y_p, z_p) and (x_d, y_d, z_d). Interestingly, in the 3D case, the computational ratio between the proposed method and the DAS technique goes up to $n_{ex}\,n_{ey}\,/\,\log(n_x\,n_y\,n_s)$, making the interest of our approach even more stronger.

V. Conclusion

In this paper, an explicit transformation for the extension of Fourier-based techniques to the reconstruction of sectorial images using DW has been presented. The key concept of the proposed formulation is based on the derivation of an isomorphism in terms of travel time between a planar system based on PW and a sectorial one based on DW. In particular, we proposed an explicit spatial transformation which allows the reconstruction of wide angle images from compounding scheme in transmission, the optimal quality of images being reached for 15 DWs (frame rate of 855 fps) on both numerical and in vitro phantoms. Results obtained from simulations and experiments revealed that the proposed extension of Lu's method produces competitive results with lower computational complexity when compared to conventional delay-and-sum technique.

ACKNOWLEDGMENT

The RF Verasonics generator was cofounded by the FEDER program, Saint-Etienne Metropole (SME) and Conseil General de la Loire (CG42) within the framework of the SonoCardio-Protection Project leaded by Pr Pierre Croisille. This work was performed within the framework of the LABEX PRIMES (ANR- 11-LABX-0063) of Université de Lyon, within the program "Investissements d'Avenir" (ANR-11-IDEX-0007) operated by the French National Research Agency (ANR). This work was also supported in part by the UltrasoundToGo RTD project (no. 20NA21 145911), evaluated by the Swiss NSF and funded by Nano-Tera.ch with Swiss Confederation financing.

References

[1] D. Vray, E. Brusseau, V. Detti, F. Varray, A. Basarab, O. Beuf, O. Basset, C. Cachard, H. Liebgott, and P. Delachartre, "Ultrasound medical imaging," *Medical Imaging Based on Magnetic Fields and Ultrasounds: John Wiley & Sons, Inc*, pp. 1–72, 2014.

[2] L. Tong, A. Ramalli, R. Jasaityte, P. Tortoli, and J. D'hooge, "Multi-transmit beam forming for fast cardiac imaging - experimental validation and in vivo application," *IEEE Transactions on Medical Imaging*, vol. 33, no. 6, pp. 1205–1219, 2014.

[3] D. Perrin, N. Vasilyev, G. Marx, and J. Pedro, "Temporal enhancement of 3d echocardiography by frame reordering," *JACC: Cardiovascular Imaging*, vol. 5, no. 3, pp. 300–304, 2012.

[4] M. Tanter and M. Fink, "Ultrafast imaging in biomedical ultrasound," *IEEE Transactions on Ultrasonics, Ferroelectrics, and Frequency Control*, vol. 61, no. 1, pp. 102–119, 2014.

[5] J. Lu, "2d and 3d high frame rate imaging with limited diffraction beams," *IEEE Transactions on Ultrasonics, Ferroelectrics and Frequency Control*, vol. 44, no. 4, pp. 839–856, July 1997.

[6] ——, "Experimental study of high frame rate imaging with limited diffraction beams," *IEEE Transactions on Ultrasonics, Ferroelectrics, and Frequency Control*, vol. 45, no. 1, pp. 84–97, 1998.

[7] J. Cheng and J. Lu, "Extended high-frame rate imaging method with limited-diffraction beams," *IEEE Transactions on Ultrasonics, Ferroelectrics, and Frequency Control*, vol. 53, no. 5, pp. 880–899, 2006.

[8] D. Garcia, L. Tarnec, S. Muth, E. Montagnon, J. Porée, and G. Cloutier, "Stolt's f-k migration for plane wave ultrasound imaging," *IEEE Transactions on Ultrasonics, Ferroelectrics and Frequency Control*, vol. 60, no. 9, pp. 1853–1867, 2013.

[9] O. Bernard, M. Zhang, F. Varray, P. Gueth, J. Thiran, H. Liebgott, and D. Friboulet, "Ultrasound fourier slice imaging: a novel approach for ultrafast imaging technique," in *IEEE International Ultrasonics Symposium (IUS)*. Ieee, 2014, pp. 129–132.

[10] G. Montaldo, M. Tanter, J. Bercoff, N. Benech, and M. Fink, "Coherent plane-wave compounding for very high frame rate ultrasonography and transient elastography," *IEEE Transactions on Ultrasonics, Ferroelectrics and Frequency Control*, vol. 56, no. 3, pp. 489–506, 2009.

[11] J. Jensen, S. Nikolov, K. Gammelmark, and M. Pedersen, "Synthetic aperture ultrasound imaging," *Ultrasonics*, vol. 44, pp. e5–e15, 2006.

[12] J. Udesen, F. Gran, K. L. Hansen, J. A. Jensen, C. Thomsen, and M. B. Nielsen, "High frame-rate blood vector velocity imaging using plane waves: simulations and preliminary experiment [12]," *IEEE Transactions on Ultrasonics, Ferroelectrics, and Frequency Control*, vol. 55, no. 8, pp. 1729–1743, 2008.

[13] J. Gennisson, T. Deffieux, E. Macé, G. Montaldo, M. Fink, and M. Tanter, "Viscoelastic and anisotropic mechanical properties of in vivo muscle tissue assessed by supersonic shear imaging," *Ultrasound in medicine & biology*, vol. 36, no. 5, pp. 789–801, 2010.

[14] J. Bercoff, G. Montaldo, T. Loupas, D. Savery, F. Mézière, M. Fink, and M. Tanter, "Ultrafast compound doppler imaging: providing full blood flow characterization," *IEEE Transactions on Ultrasonics, Ferroelectrics, and Frequency Control*, vol. 58, no. 1, pp. 134–147, 2011.

[15] J. Provost, V. Nguyen, D. Legrand, S. Okrasinski, A. Costet, A. Gambhir, H. Garan, and E. Konofagou, "Electromechanical wave imaging for arrhythmias," *Physics in medicine and biology*, vol. 56, no. 22, p. L1, 2011.

[16] M. Lenge, A. Ramalli, E. Boni, H. Liebgott, C. Cachard, and P. Tortoli, "High-frame-rate 2-d vector blood flow imaging in the frequency domain," *IEEE Transactions on Ultrasonics, Ferroelectrics, and Frequency Control*, vol. 61, no. 9, pp. 1504–1514, 2014.

[17] S. Ricci, L. Bassi, and P. Tortoli, "Real-time vector velocity assessment through multigate doppler and plane waves," *IEEE Transactions on Ultrasonics, Ferroelectrics, and Frequency Control*, vol. 61, no. 2, pp. 314–324, 2014.

[18] I. K. Ekroll, T. Dahl, H. Torp, and L. Løvstakken, "Combined vector velocity and spectral doppler imaging for improved imaging of complex blood flow in the carotid arteries," *Ultrasound in Medicine & Biology*, vol. 40, no. 7, pp. 1629–1640, 2014.

[19] I. K. Ekroll, M. M. Voormolen, O. K. V. Standal, J. M. Rau, and L. Lovstakken, "Coherent compounding in doppler imaging," *IEEE Transactions on Ultrasonics, Ferroelectrics, and Frequency Control*, vol. 62, no. 9, pp. 1634–1643, Sept 2015.

[20] S. Salles, A. Chee, D. Garcia, A. Yu, D. Vray, and H. Liebgott, "2-d arterial wall motion imaging using ultrafast ultrasound and transverse oscillations," *IEEE Transactions on Ultrasonics, Ferroelectrics, and Frequency Control*, vol. 62, no. 6, pp. 1047–1058, 2015.

[21] M. Muller, D. Ait-Belkacem, M. Hessabi, J. L. Gennisson, G. Grangé, F. Goffinet, E. Lecarpentier, D. Cabrol, M. Tanter, and V. Tsatsaris, "Assessment of the cervix in pregnant women using shear wave elastography: A feasibility study," *Ultrasound in Medicine and Biology*, vol. 41, no. 11, pp. 2789–2797, 2015.

[22] J. Provost, C. Papadacci, C. Demene, J. L. Gennisson, M. Tanter, and M. Pernot, "3-d ultrafast doppler imaging applied to the noninvasive mapping of blood vessels in vivo," *IEEE Transactions on Ultrasonics, Ferroelectrics, and Frequency Control*, vol. 62, pp. 1467–1472, 2015.

[23] D. Posada, J. Porée, A. Pellissier, B. Chayer, F. Tournoux, G. Cloutier, and D. Garcia, "Staggered multiple-prf ultrafast color doppler," *IEEE Transactions on Medical Imaging*, vol. 35, no. 6, pp. 1510–1521, 2016.

[24] J. Lu and H. Chen, "High frame rate imaging with diverging beam transmission and fourier reconstruction," in *Ultrasonics Symposium (IUS), 2011 IEEE International*, 2011, pp. 2221–2224.

[25] H. Hasegawa and H. Kanai, "High-frame-rate echocardiography using diverging transmit beams and parallel receive beamforming," *Journal of Medical Ultrasonics*, vol. 38, no. 3, pp. 129–140, 2011.

[26] C. Papadacci, M. Pernot, M. Couade, M. Fink, and M. Tanter, "High-contrast ultrafast imaging of the heart," *IEEE Transactions on Ultrasonics, Ferroelectrics and Frequency Control*, vol. 61, no. 2, pp. 288–301, 2014.

[27] J. Poree, D. Posada, A. Hodzic, F. Tournoux, G. Cloutier, and D. Garcia, "High-frame-rate echocardiography using coherent compounding with doppler-based motion-compensation," *IEEE Transactions on Medical Imaging*, vol. PP, no. 99, pp. 1–1, 2016.

[28] P. Kruizinga, F. Mastik, N. de Jong, A. van der Steen, and G. van Soest, "Plane-wave ultrasound beamforming using a nonuniform fast fourier transform," *IEEE Transactions on Ultrasonics, Ferroelectrics, and Frequency Control*, vol. 59, no. 12, pp. 2684–2691, 2012.

[29] M. Zhang, A. Besson, R. E. Carrillo, F. Varray, H. Liebgott, J. Thiran, D. Friboulet, and O. Bernard, "Extension of ultrasound fourier slice imaging theory to sectorial acquisition," in *IEEE International Ultrasonics Symposium (IUS)*, 2015.

[30] H. Stark, J. W. Woods, I. Paul, and R. Hingorani, "An investigation of computerized tomography by direct fourier inversion and optimum interpolation," *IEEE Transactions on Biomedical Engineering*, vol. BME-28, no. 7, pp. 496–505, 1981.

[31] J. D. O'Sullivan, "A fast sinc function gridding algorithm for fourier inversion in computer tomography," *IEEE Transactions on Medical Imaging*, vol. 4, no. 4, pp. 200–207, 1985.

[32] J. I. Jackson, C. H. Meyer, D. G. Nishimura, and A. Macovski, "Selection of a convolution function for fourier inversion using gridding [computerised tomography application]," *IEEE Transactions on Medical Imaging*, vol. 10, no. 3, pp. 473–478, 1991.

[33] M. V. Wijk and J. Thijssen, "Performance testing of medical ultrasound equipment: Fundamental vs. harmonic mode," *Ultrasonics*, vol. 40, pp. 585—-591, 2002.

[34] J. A. Jensen and N. B. Svendsen, "Calculation of pressure fields from arbitrarily shaped, apodized, and excited ultrasound transducers," *IEEE Transactions on Ultrasonics, Ferroelectrics, and Frequency Control*, vol. 39, no. 2, pp. 262–267, March 1992.

[35] J. A. Jensen, "Field: A program for simulating ultrasound systems," in *10TH NORDICBALTIC CONFERENCE ON BIOMEDICAL IMAGING, VOL. 4, SUPPLEMENT 1, PART 1:351–353*, 1996, pp. 351–353.

[36] B. Denarie, T. A. Tangen, I. K. Ekroll, N. Rolim, H. Torp, T. Bjåstad, and L. Lovstakken, "Coherent plane wave compounding for very high frame rate ultrasonography of rapidly moving targets," *IEEE Transactions on Medical Imaging*, vol. 32, no. 7, pp. 1265–1276, July 2013.